Available online at www.sciencedirect.com
ScienceDirect
International Journal of Heat and Mass Transfer 51 (2008) 485–496
International Journal of HEAT and MASS TRANSFER
www.elsevier.com/locate/ijhmt

Prediction of two-phase condensation in horizontal tubes using probabilistic flow regime maps

E.W. Jassim *, T.A. Newell, J.C. Chato

Department of Mechanical Science and Engineering, University of Illinois at Urbana-Champaign, 1206 West Green Street, Urbana, IL 61801, USA

Received 22 September 2006; received in revised form 22 January 2007
Available online 13 August 2007

Abstract

A flow regime based condensation model is developed for refrigerants in single, smooth, horizontal tubes utilizing a generalized probabilistic two-phase flow map. Flow map time fraction information is used to provide a physically based weighting of heat transfer models developed for different flow regimes. The developed model is compared with other models in the literature, with experimentally obtained condensation data of R134a in 8.92 mm diameter tubes, and with data found in the literature for 3.14 mm, 7.04 mm, and 9.58 mm tubes with R11, R12, R134a, R22, R410A, and R32/R125 (60/40% by weight) refrigerants and a wide range of mass fluxes and qualities.

Keywords: Condensation; Two-phase; Probabilistic; Flow regime map; Horizontal tubes

1. Introduction

Numerous two-phase condensation models are available in the literature for specific flow configurations. Recently, flow regime map based models have been developed that span multiple flow regions. The most recent of the flow regime map based models are seen to predict heat transfer for a wide range of tube sizes, fluids, and flow conditions. However, these models are difficult to implement and require interpolation to transition between flow regimes without discontinuities as a result of the flow regime maps used.

In the present study probabilistic two-phase flow map condensation models, similar to the multi-port microchannel pressure drop and void fraction models developed by Jassim and Newell [1], are developed for single, smooth, horizontal tubes in order to predict condensation heat transfer in multiple flow regimes with statistically correlated transitions. An overall condensation heat transfer coefficient is predicted as the sum of the flow regime time fractions, fractions of time that particular flow regimes are observed for given flow conditions, multiplied by representative heat transfer models for each respective flow regime. The time fractions were obtained from a generalized probabilistic two-phase flow regime map for horizontal tubes developed by Jassim [2]. Condensation heat transfer models were identified for the intermittent, stratified, and annular flow regimes. Due to the flexible nature of this model, different condensation models can be implemented. The models developed in the present study predict condensation data of R134a in 8.915 mm diameter smooth tube for a range of qualities and mass fluxes from 100 to 300 kg/(m^2 s) experimentally obtained in the present study with a mean absolute deviation of 6%. The present models developed and other flow map based condensation models in the literature are statistically compared to a database of 772 condensation points found in the literature for 3.14 mm, 7.04 mm, and 9.58 mm tubes with R11, R12, R134a, R22, R410A, and 60/40 R32/R125 by weight and a wide range of mass fluxes and qualities. Using this database the present models are found to have errors largely comparable to the models identified in the literature but

* Corresponding author. Tel.: +1 217 377 8249; fax: +1 217 333 1942.
E-mail address: jassim@uiuc.edu (E.W. Jassim).

0017-9310/$ - see front matter © 2007 Elsevier Ltd. All rights reserved.
doi:10.1016/j.ijheatmasstransfer.2007.05.021

Nomenclature

A_L	cross-sectional area of tube occupied by liquid (m^2)
C_p	specific heat (kJ/(kg K))
D	hydraulic diameter (m)
dP	pressure drop (kPa)
dz	length (m)
e	deviation (−)
e_A	mean absolute deviation (−)
e_R	average deviation (−)
F	observed time fraction (−)
fi	interfacial roughness factor (−)
Fr_{vo}	vapor only Froude number (−)
G	mass flux (kg/(m^2 s))
g_a	gravitational acceleration (9.81 m/s^2)
h	heat transfer coefficient (W/(m^2 K))
h_{lv}	latent heat of vaporization (kJ/kg)
i	intermittent flow regime curve fit constant (−)
k	thermal conductivity (W/(m K))
N	total number of data points(−)
Pr	Prandtl number (−)
Re_l	superficial liquid Reynolds number (−)
Re_{lt}	Reynolds number of the liquid film (−)
s	stratified flow regime curve fit constant (−)
T	temperature
We_{vo}	vapor only Weber number (−)
x	flow quality (−)
Xi	dimensionless group correlating the intermittent/liquid flow regime (−)
Xs	dimensionless group correlating the stratified flow regime (−)
X_{tt}	turbulent–turbulent Lockhart – Martinelli parameter (−)

Greek symbols

α	void fraction (−)
α_{ra}	predicted void fraction given by Eq. 24 (−)
δ	liquid film thickness of annular ring (m)
μ	dynamic viscosity (kg/(m s))
ρ	density (kg/m^3)
σ	surface tension (N/m)
σ_N	standard deviation
θ	upper angle of the tube not wetted by stratified liquid (radians)

Subscripts

ann	pertaining to the annular flow regime
h	homogeneous
int	pertaining to the intermittent flow regime
int + liq	pertaining to the intermittent and liquid flow regime
l	liquid
liq	pertaining to the liquid flow regime
sat	corresponding to saturation conditions
strat	pertaining to the stratified flow regime
v	vapor
vap	pertaining to the vapor flow regime
wall	at the wall

are found to improve predictions of traditional flow regime map based models in the flow regime transition regions. Consequently, probabilistic two-phase flow regime map modeling is a promising new modeling technique for condensation heat transfer and will allow pressure drop and void fraction to be modeled with the same flow regime based time fraction information.

2. Literature review

Numerous two-phase flow condensation models can be found in the literature, and most of these models can be categorized as stratified flow or annular flow models. The Chato [3] stratified flow model considers film condensation at the top of the tube and neglects the vapor shear driven condensation at the bottom of the tube because the bottom liquid layer is assumed to be thick. Jaster and Kosky [4] modified the Chato [3] model by introducing void fraction to account for liquid pool depth variation, but also neglects heat transfer in the liquid pool. This modification is reported by Dobson and Chato [5] to negatively effect the heat transfer predictions in the stratified flow regime. Rosson and Meyers [6] developed a model for condensation of acetone and methanol in the stratified and slug plug flow regimes which considered both film condensation and vapor shear driven condensation.

Annular flow heat transfer models can be further divided into two-phase multiplier based, shear based, and boundary layer based models. Two-phase multiplier models often resemble a modified Dittus–Boelter [7] relation such as the condensation models by Akers et al. [8], Shah [9], Cavallini and Zecchin [10], Bivens and Yokozeki [11], and Tang [12]. Shear based models were originally developed by Carpenter and Colburn [13] which was subsequently modified by Soliman et al. [14] who's model was then modified by Chen et al. [15]. Examples of boundary layer correlation based heat transfer models can be found in Traviss et al. [16], Cavallini and Zecchin [10] and Hurlburt and Newell [17]. All of the above models tend to predict heat transfer most accurately in the flow regime for which they were derived.

Recently, flow regime map based two-phase flow heat transfer models were developed in order to predict condensation heat transfer in multiple flow regimes. Haraguchi et al. [18] and Dobson and Chato [5] developed flow regime map based two-phase flow condensation heat

transfer models for multiple flow regimes. Dobson and Chato [5] modeled heat transfer in both the stratified wavy and annular flow regimes. They used a two-phase multiplier approach in developing their annular flow model component. Dobson and Chato's [5] stratified wavy model component accounted for both forced convective condensation at the bottom of the tube and film condensation at the top of the tube. They used Soliman's [19] flow map to determine the transition between stratified wavy and annular flow. Cavallini et al. [20] then developed a flow regime map based condensation model and validated it with over 2000 data points consisting of 9 different refrigerants in 3.1–21.4 mm diameter tubes. Cavallini et al. [20] accounted for annular, stratified, and slug flow in their model. They developed an interfacial shear based condensation model for the annular flow regime, a stratified flow model that includes both film and convective condensation, and a slug flow regime model. The transitions between some of the models were determined through an interpolation between the flow regimes. Thome et al. [21] created a model with less empirical constants and avoids heat transfer jumps across flow regime boundaries that occur in the Dobson and Chato [5] and in the slug flow regime transition in the Cavallini et al. [20] model. Thome et al. [21] includes models for the intermittent, fully stratified, stratified wavy, annular, and mist flow regimes. The annular flow regime model developed is used for intermittent and mist flow regimes. Thome et al. [21] uses flow transition criteria from a Steiner [22] style flow map for condensation conditions, which is developed by El Hajal et al. [23] as a modification of the flow map developed by Kattan et al. [24] for flow boiling in horizontal tubes. Their model includes the effects of liquid vapor interfacial roughness for annular flow and considers both film and convective condensation effects in the stratified wavy and fully stratified flow regimes. Interpolations are used between flow regime boundaries to provide continuous transitions. Thome et al. [21] compared their flow map based heat transfer model with a large condensation database of 15 different fluids that includes 1850 refrigerant data points and 2771 hydrocarbon data points. Cavallini et al. [25] then revised their Cavallini et al. [20] model to eliminate the discontinuity in the slug flow regime transition.

All of the flow regime map based heat transfer models mentioned utilize traditional Steiner [22] or Taitel and Dukler [26] type flow regime maps which indicate a particular flow regime at a given quality and mass flux. The distinct lines seem to lack a physical basis as Coleman and Garimella [27], El Hajal et al. [23], and Niño [28] indicate that more than one flow regime can exist near the boundaries or within a given flow regime on a Steiner [22] type flow map. Traditional flow maps such as Mandhane [29], Steiner [22], and Taitel and Dukler [26] type flow maps can not be represented as continuous functions for the entire quality range as can be seen from a Steiner [22] type flow map in Fig. 1. Consequently, these heat transfer models tend to be complicated with an interpolation scheme to avoid discontinuities at the flow regime boundaries.

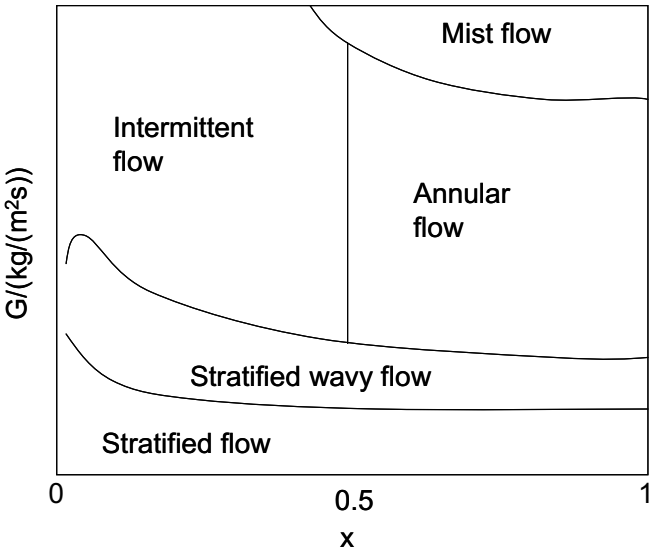

Fig. 1. Steiner [22] type flow map depiction.

Probabilistic two-phase flow regime maps first developed by Niño [28] for refrigerant and air-water flow in multi-port microchannels are found by Jassim and Newell [1] to eliminate the discontinuities created by traditional flow maps. Probabilistic two-phase flow regime maps have quality on the horizontal axis and the "fraction of time", F, in which a particular flow regime is observed in a series of pictures taken at given flow condition on the ordinate as seen in Fig. 2. Jassim and Newell [1] developed continuous curve fit functions to represent the data, obtained by Niño [28] for 6-port microchannels, for the entire quality range with correct physical limits. Jassim and Newell [1] then utilized the probabilistic flow regime map time fraction curve fits to predict pressure drop and void fraction as shown in Eqs. (1) and (2), respectively.

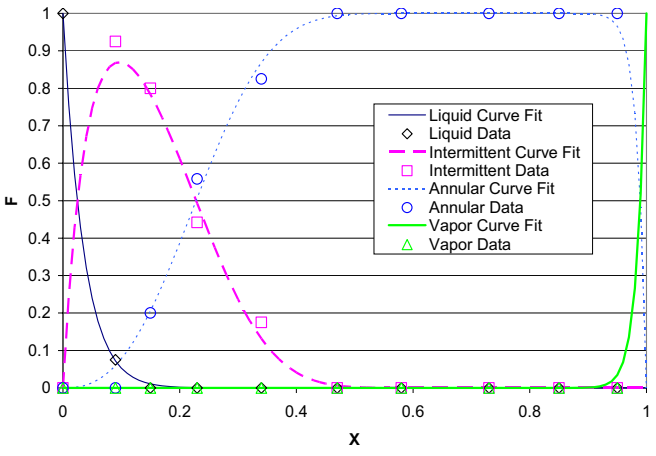

Fig. 2. Probabilistic flow map with time fraction curve fits for R410A, 10 °C, 300 kg/(m^2 s) in a 6-port 1.54 mm hydraulic dia. microchannel taken from Jassim and Newell [1].

$$\left(\frac{dP}{dz}\right)_{total} = F_{liq}\left(\frac{dP}{dz}\right)_{liq} + F_{int}\left(\frac{dP}{dz}\right)_{int} + F_{vap}\left(\frac{dP}{dz}\right)_{vap} + F_{ann}\left(\frac{dP}{dz}\right)_{ann} \quad (1)$$

$$\alpha_{total} = F_{liq}\alpha_{liq} + F_{int}\alpha_{int} + F_{vap}\alpha_{vap} + F_{ann}\alpha_{ann} \quad (2)$$

Jassim [2] then developed probabilistic two-phase flow maps for single tubes with the experimentally obtained time fraction data from Jassim et al. [30] who utilized the flow loop depicted in Fig. 3. Jassim [2] developed curve fits for the intermittent/liquid, stratified, and annular flow regime time fraction data. The time fraction functions are given in Eqs. (3)–(5) for the intermittent/liquid, stratified, and annular flow regimes, respectively.

$$F_{int+liq} = (1-x)^i \quad (3)$$

$$F_{strat} = (1-x^{(s/\sqrt{x})})^i - (1-x)^i \quad (4)$$

$$F_{ann} = 1 - F_{int+liq} - F_{strat} \quad (5)$$

The flow maps developed were generalized by linking the time fraction curve fit constants to physical parameters. The intermittent/liquid time fraction curve fit constant "*i*", given in Eq. (6), has a linear relationship with the dimensionless group *Xi*, given in Eq. (7), which contains the vapor only Webber number, given in Eq. (8), and the liquid to vapor density ratio.

$$i = 0.0243Xi + 8.07 \quad (6)$$

$$Xi = (We_{vo}^{0.4})\left(\frac{\rho_l}{\rho_v}\right), \text{where} \quad (7)$$

$$We_{vo} = \left(\frac{G^2 D}{\rho_v \sigma}\right) \quad (8)$$

The stratified time fraction curve fit constant "*s*", given in Eq. (9), has a strong relationship with the dimensionless group *Xs*, given in Eq. (10), which contains the square root of the vapor only Froude number, given in Eq. (11), and the vapor to liquid density ratio.

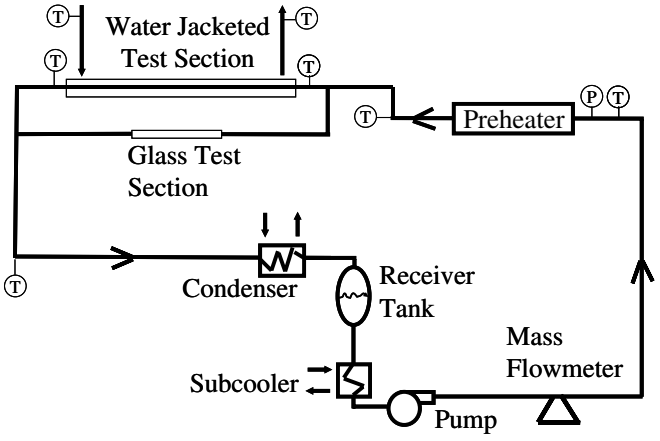

Fig. 3. Two-phase flow loop schematic.

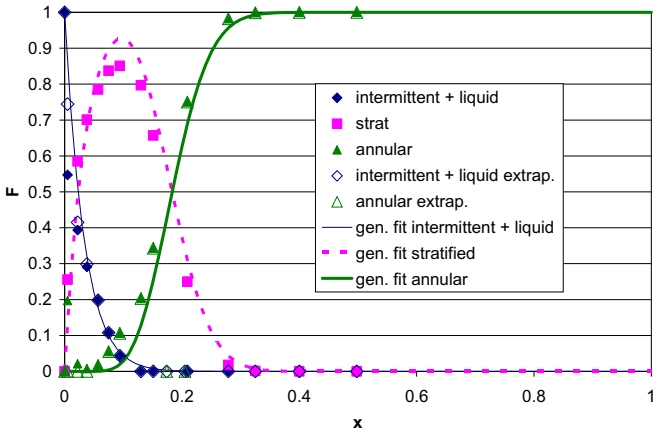

Fig. 4. Probabilistic flow map with generalized time fraction curve fits for 8.00 mm diameter tube, R134a, 25 °C, 300 kg/(m^2 s).

$$s = \frac{1}{0.45Xs} + \frac{1}{0.025Xs^{4.44}} \quad (9)$$

$$Xs = (Fr_{vo}^{0.5})\left(\frac{\rho_v}{\rho_l}\right)^{0.65} \quad (10)$$

$$Fr_{vo} = \left(\frac{G^2}{\rho_v^2 g_a D}\right) \quad (11)$$

A sample probabilistic two-phase flow regime map with generalized curve fits is depicted in Fig. 4 for 8.00 mm diameter tube with R134a flowing at 25 °C and 300 kg/(m^2 s). Jassim [2] found these generalized curve fit constants to represent the time fraction data for horizontal 8.00 mm, 5.43 mm, and 3.90 mm diameter tubes with an average absolute error of 0.022, 0.094, and 0.071 for the intermittent/liquid, stratified, and annular flow regimes, respectively. The average absolute error for the 1.74 mm diameter tube in the intermittent flow regime is reported to be 0.044, with the same error for the annular flow regime if the stratified flow regime is neglected, which is not observed for this tube diameter.

3. Heat transfer data

Heat transfer data was experimentally obtained using the two-phase flow loop facility at the University of Illinois Air Conditioning and Refrigeration Center depicted in Fig. 3. The liquid refrigerant is pumped with a gear pump that is driven by a variable frequency drive from the bottom of a 2 L receiver tank through a water cooled shell and tube style subcooler in order to avoid pump cavitation. The liquid refrigerant then travels through a Coriolis style mass flow meter with an uncertainty of ±0.1% followed by a preheater used to reach the desired quality. The preheater consists of a finned tube heat exchanger with opposing electric resistance heater plates bolted on either side of the heat exchanger. The electric heaters are controlled with on/off switches and a variable auto transformer to provide fine adjustment of quality. This preheater design has sufficient thermal mass to avoid "burn-out" at a quality of 100%

and has a small enough thermal mass so that steady state conditions can be rapidly attained. The refrigerant is then directed through 90° bends to remove effects of heat flux from the preheater, such as dryout, before it reaches the test section. The refrigerant can be directed either through the flow visualization test section, used by Jassim et al. [30], or a heat transfer test section used in the present study. Finally, the refrigerant is condensed in a water cooled brazed plate heat exchanger and is directed back into the receiver tank. The pressure before the inlet of the preheater is measured by a pressure transducer with an uncertainty of ±1.9 kPa. The temperatures before the inlet of the preheater and the test section are measured with type T thermocouples. These pressures and temperatures are used to determine the thermodynamic states necessary to compute the test section inlet quality. An energy balance was performed by heating single-phase fluid in the preheater and measuring the temperature difference across it along with the flow rate to determine a ±0.8% uncertainty associated with the preheater power input.

The test section consists of a 8.915 mm I.D. smooth copper tube with 4 stations of 4 thermocouples welded on the walls and a clear PVC water jacket as seen in Fig. 5. The wall temperature is determined as the average of the 16 thermocouples welded on the tube wall. Insulation is placed on the outside of the water jacket. The test section is cooled with water supplied from a water conditioner at 15.7 °C. Thermocouples are placed at the inlet and outlet of the test section in order to determine the average refrigerant temperature. A flow meter is placed in the water jacket loop and thermocouples are placed at the inlet and exit of the test section water jacket in order to determine the heat lost by the copper tube test section. A mixing section consisting of a collapsed plastic net is placed in the water flow stream at the exit of the test section to ensure that the average water temperature is measured. After the test section, the refrigerant is condensed in a flat plate heat exchanger with cold water at 5 °C. The test section saturation temperature is controlled by varying the flow rate of the cold water entering the flat plate condenser. All of the thermocouples in the test section and flow loop are type T with an uncertainty of ±0.1 °C (confirmed using an RTD with an uncertainty of ± 0.01 °C). Single-phase heat transfer tests are conducted to verify that the experimental apparatus is working properly. The single-phase heat transfer coefficients for heated sub-cooled liquid R134a in 8.915 mm diameter smooth copper tube at different mass fluxes can be observed in Fig. 6 along with the Dittus–Boelter single-phase heat transfer correlation. From this figure it can be seen that the data has good agreement with the Dittus–Boelter correlation with all of the predicted points within the experimental uncertainty. The heat flux varied in Fig. 6 which explains the scatter of the data at the low mass flux range. A waterside and refrigerant side energy balance was performed on the single-phase tests yielding a maximum error of 5%. All measurements in the present study represent the average of approximately 50 measurements taken at 3 s intervals by a data acquisition system.

Condensation heat transfer measurements were obtained for R134a at a 25 °C saturation temperature in a smooth 8.915 mm diameter copper tube with heat fluxes ranging from 4600 to 5600 W/m^2 and mass fluxes of 100, 200, and 300 kg/(m^2 s) as seen in Figs. 7–9, respectively. The heat transfer coefficient measurements are average values since there is a change of quality from the inlet to the outlet of the test section. However, the average change in quality between the inlet and outlet of the test section is small, approximately 0.09 (0.15 for Fig. 7, 0.075 for Fig. 8, and 0.5 in Fig. 9), which allows for comparison to local heat transfer values. The uncertainty in average quality is found to be less than ±1% for all the data in Figs. 7–9. The average mass flux is found to be within

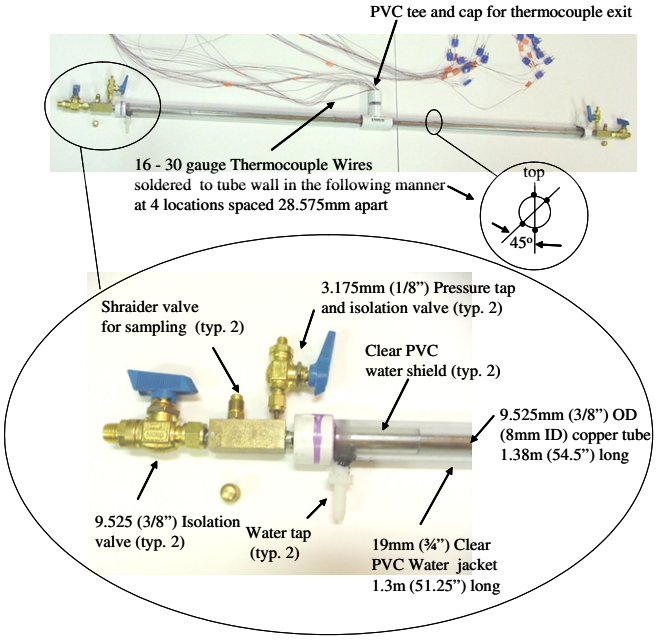

Fig. 5. Heat transfer test section design.

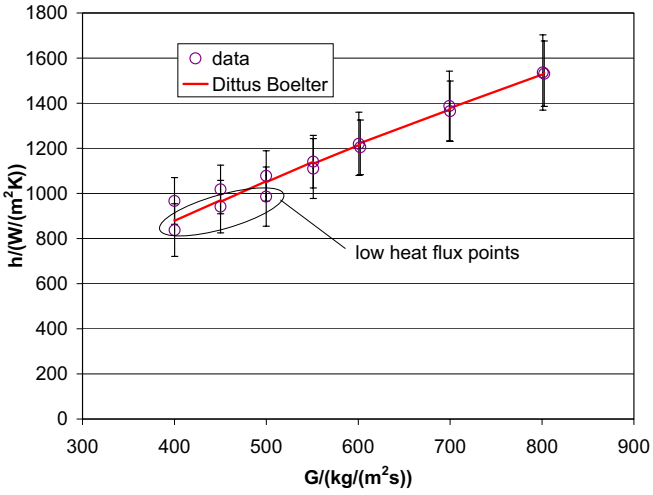

Fig. 6. Sub-cooled liquid R134a heat transfer in 8.915 mm diameter smooth tube with heat addition varying from 2600 to 5600 W/(m^2).

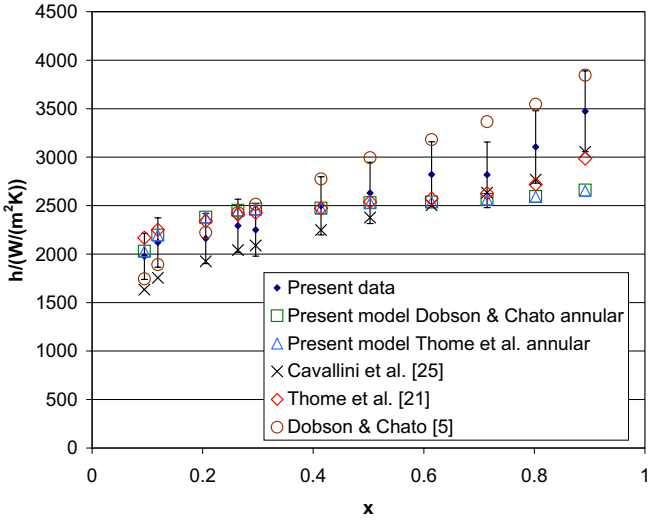

Fig. 7. Average quality vs. condensation heat transfer coefficients for R134a, 25 °C, 100 kg/(m^2 s), in 8.915 mm I.D. smooth tube, 4600–5400 W/m^2.

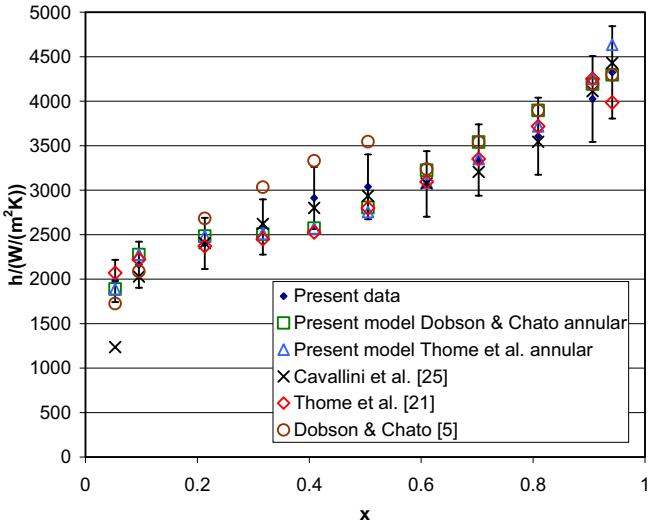

Fig. 8. Average quality vs. condensation heat transfer coefficients for R134a, 25 °C, 200 kg/(m^2 s), in 8.915 mm I.D. smooth tube, 4700–5600 W/m^2.

±1% of the values reported in Figs. 7–9. The heat flux varied because the cooling water temperature was held constant. From Figs. 7–9 it can be seen that the experimental data agrees well with the models presented by Dobson and Chato [5], Cavallini [20], Thome et al. [21], and the probabilistic flow map based models developed in the present study with different annular flow models used. The models are represented as points, instead of curves, since the heat flux and mass flux varied from point to point.

4. Probabilistic two-phase flow map condensation model

A probabilistic two-phase flow map condensation model is formulated for tubes in a similar manner as was formulated for pressure drop and void fraction in microchannels by Jassim and Newell [1] in Eqs. (1) and (2), respectively. The probabilistic two-phase flow map condensation model given in Eq. (12) is simply the sum of the time fraction for each flow regime multiplied by a model developed for its respective flow regime.

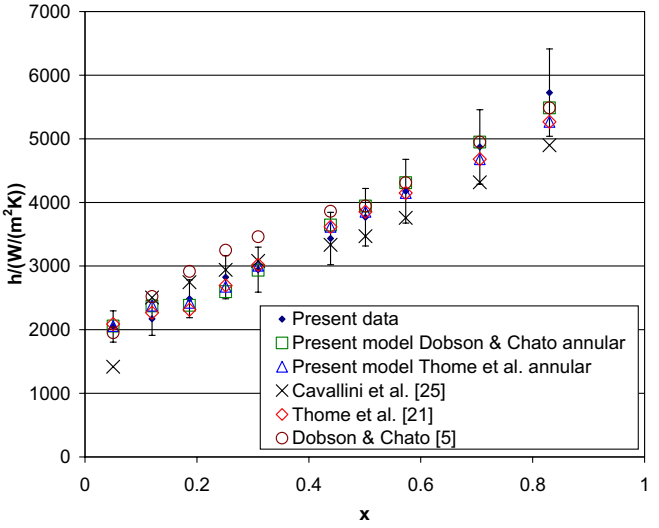

Fig. 9. Average quality vs. condensation heat transfer coefficients for R134a, 25 °C, 300 kg/(m^2 s), in 8.915 mm I.D. smooth tube, 4700–5500 W/m^2.

$$h_{\text{total}} = F_{\text{int+liq}} h_{\text{int+liq}} + F_{\text{strat}} h_{\text{strat}} + F_{\text{ann}} h_{\text{ann}} \tag{12}$$

In this way the model applies the appropriate assumptions (flow regime information) in a quantitative and explicit manner for a full range of flow conditions. This model is flexible in that different heat transfer models can be chosen for a given flow regime. Furthermore, it allows for pressure drop, void fraction, and heat transfer to be modeled on a consistent flow regime time fraction weighted basis. Simple heat transfer models are developed or identified for each flow regime in the subsequent model description in order to illustrate the effectiveness and flexibility of this modeling technique, and to illustrate how this modeling technique is able to compliment heat transfer models found in the literature.

4.1. Intermittent/liquid flow regime condensation model

A condensation model based on a modified Dittus–Boelter relation, given in Eq. (13), is developed for the intermittent/liquid flow regime.

$$h_{\text{int+liq}} = 0.023 \left(\frac{k_l}{D}\right) \left(\frac{GD}{\mu_l}\right)^{0.8} Pr_l^{0.3}, \text{where} \tag{13}$$

$$Pr_l = \frac{\mu_l C_{pl}}{k_l} \tag{14}$$

The Dittus–Boelter equation which was developed for turbulent single-phase flow is modified by using the two-phase mass flux while using the liquid refrigerant properties. This model assumes that the vapor phase is not contributing to

the heat transfer other than the fact that it is a contributor to the total mass flux. As the quality approaches zero, Eq. (13) approaches the Dittus–Boelter equation which is the correct physical limit.

4.2. Stratified flow regime condensation model

The Chato [3] model, given in Eq. (15), is utilized for the stratified flow regime.

$$h_{\text{strat}} = 0.555\left(\frac{k_l}{D}\right)\left(\frac{\rho_l(\rho_l-\rho_v)gh_{lv}D^3}{k_l\mu_l(T_{\text{sat}}-T_{\text{wall}})}\right)^{0.25} \tag{15}$$

This model is used because it is simple and gives reasonable heat transfer results in the stratified flow regime.

4.3. Annular flow regime condensation model

Two different simple, yet accurate, annular flow regime models found in the literature were used to represent h_{ann} in the present model for illustration purposes. The Dobson and Chato [5] two-phase multiplier based heat transfer model for annular flow, given in Eq. (16), is used to represent h_{ann}.

$$h_{\text{ann}} = 0.023\left(\frac{k_l}{D}\right)Re_l^{0.8}Pr_l^{0.4}\left(1+\frac{2.22}{X_{tt}^{0.889}}\right), \text{where} \tag{16}$$

$$X_{tt} = \left(\frac{1-x}{x}\right)^{0.9}\left(\frac{\rho_v}{\rho_l}\right)^{0.5}\left(\frac{\mu_l}{\mu_v}\right)^{0.1}, \text{and} \tag{17}$$

$$Re_l = \frac{GD(1-x)}{\mu_l} \tag{18}$$

The annular portion of the more recently developed Thome et al. [21] model, which was verified with a wide range of refrigerant and hydrocarbon properties and tube sizes, is also used to represent h_{ann} in the present model. The Thome et al. [21] annular flow, given in Eqs. (19)–(26), is more complicated than that of Dobson and Chato [5].

$$h_{\text{ann}} = 0.003Re_{lt}^{0.74}Pr_l^{0.5}\frac{k_l}{\delta}f_i \tag{19}$$

$$f_i = 1+\left(\frac{u_v}{u_l}\right)^{0.5}\left(\frac{(\rho_l-\rho_v)g_a\delta^2}{\sigma}\right)^{0.25} \tag{20}$$

$$Re_{lt} = \frac{4G(1-x)\delta}{(1-\alpha)\mu_l} \tag{21}$$

$$\delta = 0.5D - 0.5\left(D^2-\frac{8A_L}{2\pi-\theta}\right)^{0.5}, \text{ where } \theta = 0 \text{ for annular flow} \tag{22}$$

$$A_L = \frac{\pi D^2}{4}(1-\alpha) \tag{23}$$

$$\alpha_{ra} = \frac{x}{\rho_v}\left[(1+0.12(1-x))\left(\frac{x}{\rho_v}+\frac{1-x}{\rho_l}\right)+\frac{1.18(1-x)[g_a\sigma(\rho_l-\rho_v)]^{0.25}}{G\rho_l^{0.5}}\right]^{-1} \tag{24}$$

$$\alpha_h = \left[1+\left(\frac{1-x}{x}\right)\left(\frac{\rho_v}{\rho_l}\right)\right]^{-1} \tag{25}$$

$$\alpha = \frac{\alpha_h-\alpha_{ra}}{\ln\left(\frac{\alpha_h}{\alpha_{ra}}\right)} \tag{26}$$

5. Probabilistic two-phase flow map condensation model evaluation

The probabilistic two-phase flow map condensation models developed in the present paper are compared with data from the present study, Dobson [31], and Sacks [32] summarized in Table 1, and with models developed in the literature. The present model predictions using the Thome et al. [21] annular flow model and using the Dobson and Chato [5] annular flow model, the Dobson and Chato [5] model, the Cavallini et al. [25] model, and the Thome et al. [21] model predictions are plotted with the present average heat transfer data in Figs. 7–9 for 100, 200, and 300 kg/(m^2 s) mass fluxes, respectively. These figures indicate that the present models perform well when compared to the present data and flow regime map based models in the literature. Fig. 10 compares the local heat transfer coefficient predictions of R134a at 35 °C flowing through smooth 9 mm diameter tube at 200 kg/(m^2 s) with $T_{\text{sat}} - T_{\text{wall}} = 2$ °C for the present model using the Thome et al. [21] annular flow model with the flow regime based models of Cavallini et al. [25] and Thome et al. [21] for qualities near 0 to 1. This figure indicates that the physically based transitions of present probabilistic model smoothes the transitions from one flow regime to the next.

The present model using the Thome et al. [21] annular flow model and using the Dobson and Chato [5] annular flow model, the Dobson and Chato [5] model, the Cavallini et al. [25] model, and the Thome et al. [21] model predictions are plotted versus the experimental data summarized in Table 1 for R11, R12, R134a, R22, R410A, R32/R125 (60/40% by mass) in Figs. 11–16, respectively. The experimental data summarized in Table 1 are average heat transfer values but have relatively small changes in quality between inlet and outlet which allows for comparison with the local heat transfer coefficient predictions. All of the heat transfer data summarized in Table 1 is two-phase with no superheated or sub-cooled inlet or outlet conditions. The average difference in inlet to outlet quality and saturation temperature and the average values of $T_{\text{sat}} - T_{\text{wall}}$ are given in Table 1 for each source. Fig. 17 depicts a plot of all of the refrigerant data versus the predictions of the present models along with the models of Dobson and Chato [5], Cavallini et al. [25], and Thome et al. [21]. From these figures it can be seen that all five models represent the data well. However, there seems to be a systematic over prediction of the highest pressure R32/R125 (60/40% by weight) refrigerant data by the Dobson and Chato [5] model which was also noted by Cavallini et al. [25]. As a result, the present model using the Dobson and Chato [5] annular flow

Table 1
Condensation data pool used to compare the present models with other models in the literature

Source	D/(mm)	Refrigerants	G/(kg/(m^{2}s))	T_{sat}/(°C)	$(T_{sat}-T_{wall})$/(°C)	Average $(T_{sat}-T_{wall})$/(°C)	Average $x_{in}-x_{out}$	Average $(T_{sat\_in}-T_{sat\_out})$/(°C)	Data points
Dobson [31]	3.14, 7.04	R134a, R22, R410A, R32(60%)/R125(40%) by mass	24–812	33.5–46.4	1.1–8.8	3.16	0.20	0.14	619
Sacks [32]	9.576	R11, R12, R22	84–902	25.9–31.9	0.7–9.9	2.96	0.15	0.46	121
Present study	8.915	R134a	100–300	24.9–25.1	1.0–2.4	1.79	0.09	0.25	32

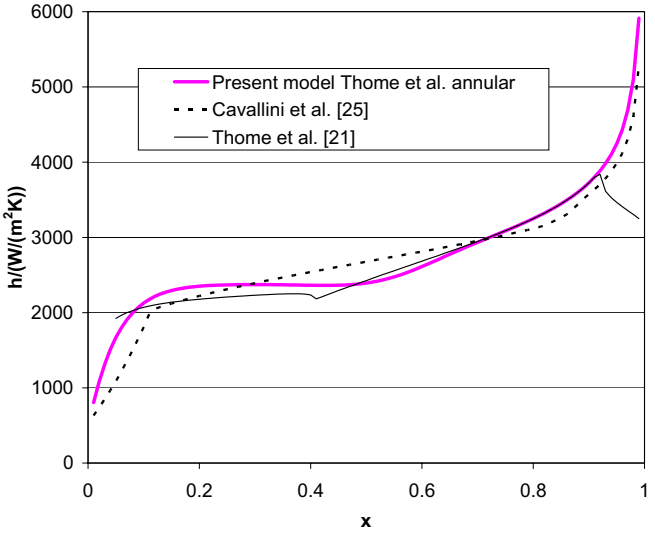

Fig. 10. Local quality vs. predicted condensation heat transfer coefficients for R134a, 35 °C, 200 kg/(m^2 s), in 9.0 mm I.D. smooth tube, $T_{sat}-T_{wall}=2$°C.

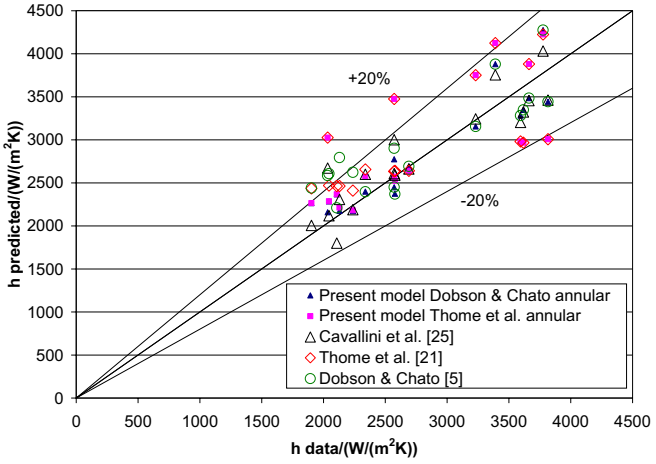

Fig. 11. Experimental vs. predicted condensation heat transfer for R11 data outlined in Table 1.

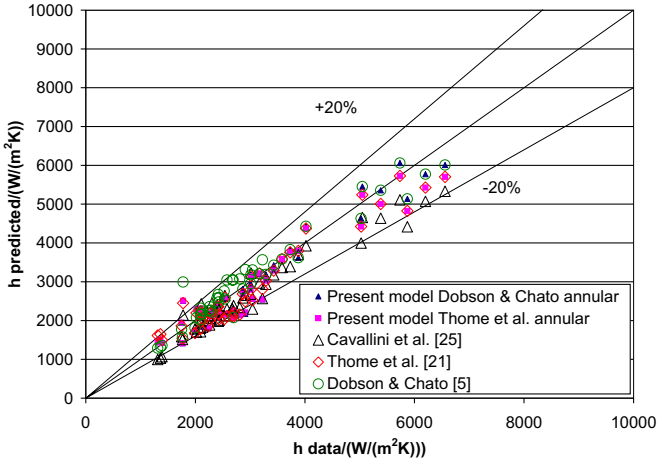

Fig. 12. Experimental vs. predicted condensation heat transfer for R12 data outlined in Table 1.

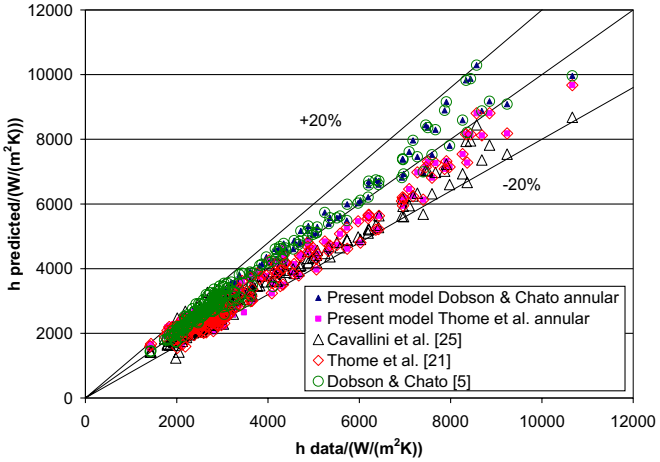

Fig. 13. Experimental vs. predicted condensation heat transfer for R134a data outlined in Table 1.

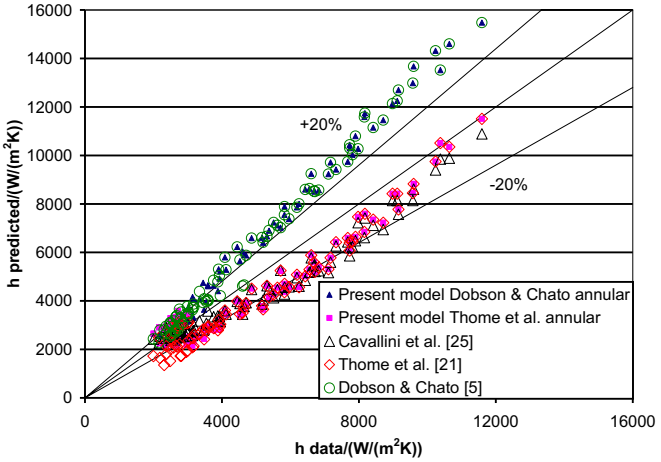

Fig. 16. Experimental vs. predicted condensation heat transfer for R32/R125 (60/40% by weight) data outlined in Table 1.

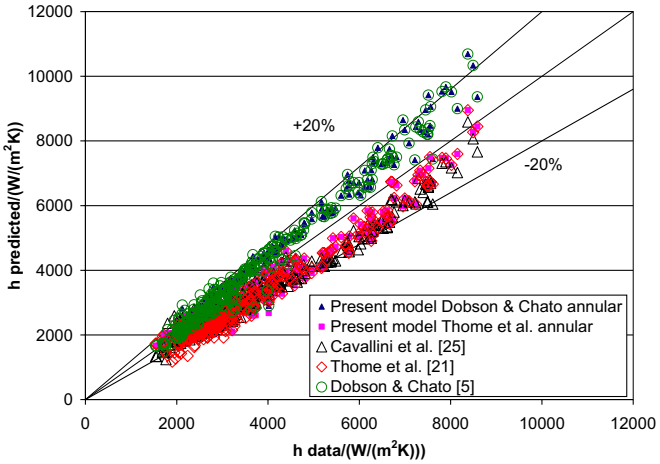

Fig. 14. Experimental vs. predicted condensation heat transfer for R22 data outlined in Table 1.

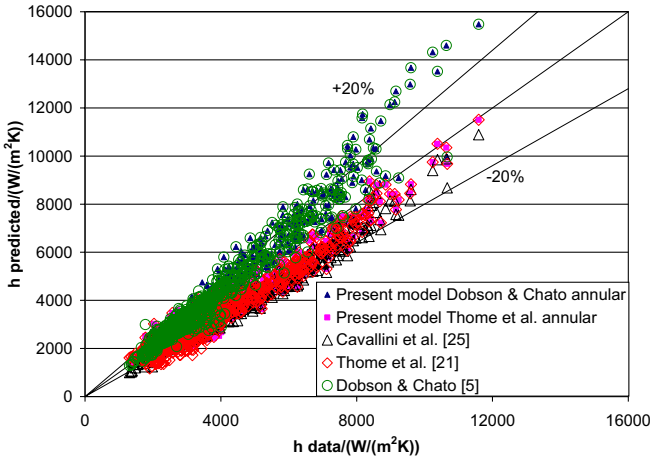

Fig. 17. Experimental vs. predicted condensation heat transfer for all data outlined in Table 1.

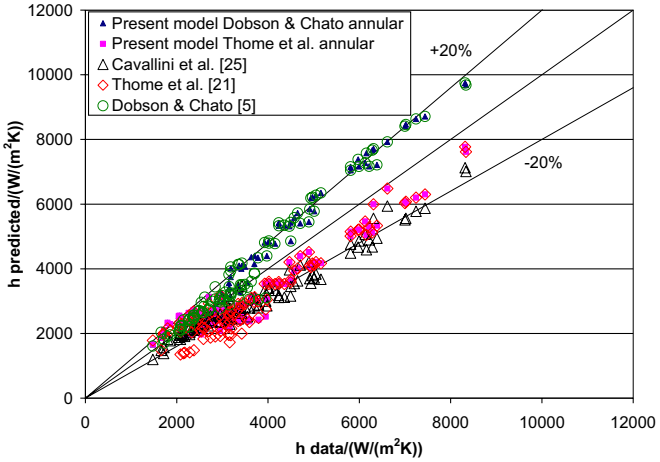

Fig. 15. Experimental vs. predicted condensation heat transfer for R410A data outlined in Table 1.

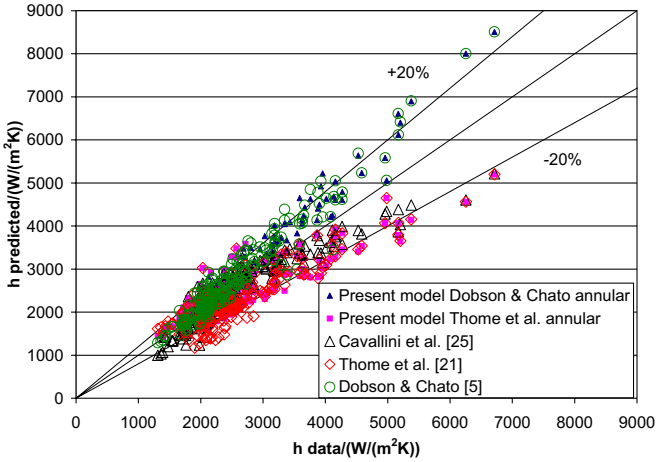

Fig. 18. Experimental vs. predicted condensation heat transfer for all data outlined in Table 1 below a quality of 0.30 (210 data points).

model is also seen to over predict the R32/R125 (60/40% by weight) data. The predicted versus measured heat transfer coefficients for qualities less than 30% is given in Fig. 18 to indicate how the present probabilistic flow map based models perform relative to traditional flow regime map based models found in the literature in a region where the flow regime transitions are most prominent. Fig. 18 indicates that the present probabilistic flow regime map based models largely improve the heat transfer predictions of the Thome et al. [21] and Dobson and Chato [5] models. Little difference is seen between heat transfer coefficient predictions above 4000 W/(m^2 K) because these predictions correspond to mostly annular flow (annular flow regime time fraction at or near 1) where the respective probabilistic and traditional flow regime map based models converge.

A statistical comparison of the present models, the Dobson and Chato [5] model, the Cavallini et al. [25] model, and the Thome et al. [21] model with all of the data detailed in Table 1 is summarized in Table 2. Table 2 contains the mean absolute deviation, e_A, the average deviation, e_R, and the standard deviation, σ_N, given in Eqs. (27)–(29), respectively, along with the percentage of predicted points lying with in ±20% error bars.

$$e_A = \frac{1}{N}\sum 100\left|\frac{h_{pred} - h_{data}}{h_{data}}\right| \tag{27}$$

$$e_R = \frac{1}{N}\sum 100\left(\frac{h_{pred} - h_{data}}{h_{data}}\right) \tag{28}$$

$$\sigma_N = \left[\frac{1}{N-1}\sum (e - e_R)^2\right]^{0.5} \text{ where, } e = 100\left(\frac{h_{pred} - h_{data}}{h_{data}}\right) \tag{29}$$

It is evident from Table 2 that the present probabilistic two-phase flow map based condensation models are comparable to the models presented by Dobson and Chato [5], Cavallini et al. [25], and Thome et al. [21] when compared to the present data set. The present condensation model using the Thome et al. [21] model is seen to have less deviation than the present condensation model using the Dobson and Chato [5] annular flow model for the high pressure R32/R125 (60/40% by weight) data as observed in Fig. 16.

Table 2
Statistical comparison of condensation models with experimental data using different refrigerants (in %)

Refrigerant	Statistical comparison	Present model Thome et al. annular	Present model Dobson Chato annular	Thome et al. [21]	Cavallini et al. [25]	Dobson Chato [5]
R11	e_A	14.4	7.7	17.0	8.2	12.5
	e_R	7.5	2.3	10.5	2.5	7.4
	σ_N	17.8	9.1	18.2	11.1	14.4
	within 20%	77.8	100.0	66.7	94.4	77.8
R12	e_A	10.4	9.7	10.7	12.9	7.6
	e_R	−5.1	−3.9	−5.0	−10.7	3.1
	σ_N	12.4	12.4	12.4	9.7	12.4
	within 20%	87.5	89.6	87.5	83.3	95.8
R134a	e_A	10.7	8.2	9.9	10.7	6.4
	e_R	−6.4	0.9	−6.9	−8.3	4.2
	σ_N	10.8	10.0	9.5	9.0	7.0
	within 20%	91.8	95.4	93.6	95.9	99.1
R134a (Present data only)	e_A	6.0	6.2	5.5	9.3	10.1
	e_R	−1.1	−0.6	−1.1	−6.8	7.0
	σ_N	7.9	7.9	6.7	12.5	11.6
	within 20%	96.9	96.9	100.0	93.8	100.0
R22	e_A	12.9	11.8	14.4	13.2	10.3
	e_R	−10.8	5.7	−13.1	−11.3	8.3
	σ_N	10.0	12.0	9.7	9.3	9.1
	within 20%	84.0	90.4	79.5	85.7	90.4
R410A	e_A	15.8	15.3	17.9	16.1	12.3
	e_R	−10.3	9.2	−14.6	−16.0	10.4
	σ_N	14.3	14.4	14.4	7.9	10.7
	within 20%	77.9	67.3	72.1	62.5	72.1
R32/R125 60/40% by mass	e_A	18.2	26.6	18.0	13.6	24.6
	e_R	−9.7	26.6	−16.1	−11.1	24.6
	σ_N	17.4	9.6	12.3	10.8	10.8
	within 20%	57.8	21.1	60.0	76.7	28.9
All refrigerants	e_A	13.2	12.7	13.8	12.8	11.0
	e_R	−8.6	6.6	−10.9	−10.7	9.0
	σ_N	12.6	14.0	12.1	9.8	11.2
	within 20%	82.4	80.8	80.4	84.5	83.3

6. Conclusion

In summary, probabilistic two-phase flow map heat transfer models are developed for single, smooth, horizontal, tubes in a similar manner as pressure drop and void fraction models with a common flow map prediction basis. Previously developed generalized probabilistic two-phase flow regime maps in tubes are utilized in the present condensation models. The probabilistic two-phase flow map heat transfer model weights the importance of the intermittent, stratified, and annular flow regimes based on the time fraction functions which provide smooth, physically based transitions. The present model has the flexibility to accept different models developed for each flow regime as more accurate models are identified. Condensation models were identified in the literature or developed for each flow regime based on their accuracy and simplicity. The present models are compared with condensation data with R134a in 8.915 mm I.D. smooth, adiabatic, horizontal tube experimentally obtained in the present study and with flow map based models found in the literature with good agreement (mean absolute deviation of 6% with the present models). Furthermore, the present probabilistic flow map models developed and flow map based models found in the literature are compared with 772 condensation data points, found in the literature, with good agreement. The present models using the Thome et al. [21] and the Dobson and Chato [5] annular flow components are found to have a mean absolute deviation of 13.2% and 12.7%, respectively, which is largely comparable to the 13.8%, 12.8%, and 11.0% mean absolute deviation of the models by Thome et al. [21], Cavallini et al. [25], and the Dobson and Chato [5], respectively. However, the probabilistic model using the Dobson and Chato [5] annular flow component is found to over predict high pressure R32/R125 (60/40% by weight) data. The present probabilistic flow regime map base technique is found to improve predictions of traditional flow regime map based models in the flow regime transition regions. Caution must be exercised in using the present models outside of the range of tube diameters, refrigerant properties and flow conditions with which it is presently compared.

Acknowledgements

The authors thank the Air Conditioning and Research Center (ACRC) at the University of Illinois for their financial support. The authors would also like to thank Matthew Alonso, Frank Lam, Sarah Brewer, and Kin Lai for aiding in the heat transfer data acquisition, and Ben Newell for aiding in the design of the two-phase flow loop.

References

[1] E.W. Jassim, T.A. Newell, Prediction of two-phase pressure drop and void fraction in microchannels using probabilistic flow regime mapping, Int. J. Heat Mass Transfer 49 (2006) 2446–2457.

[2] E.W. Jassim, Probabilistic Flow Regime Map Modeling of Two-phase Flow, Ph.D. Thesis, University of Illinois, Urbana-Champaign, IL, 2006.

[3] J.C. Chato, Laminar condensation inside horizontal and inclined tubes, ASHRAE J. 4 (1962) 52–60.

[4] H. Jaster, P.G. Kosky, Condensation in a mixed flow regime, Int. J. Heat Mass Transfer 19 (1976) 95–99.

[5] M.K. Dobson, J.C. Chato, Condensation in smooth horizontal tubes, J. Heat Transfer 120 (1998) 193–213.

[6] H.F. Rosson, J.A. Myers, Point values of condensing film coefficients inside a horizontal tube, Chem. Eng. Progress Symp. Ser. 61 (59) (1965) 190–199.

[7] F.W. Dittus, L.M.K. Boelter, Heat transfer in automobile radiators of the tubular type, Univ. California Publ. Eng. 2 (1930) 443–461.

[8] W.W. Ackers, H.A. Deans, O.K. Crosser, Condensation heat transfer within horizontal tubes, Chem. Eng. Prog. Symp. Ser. 55 (1959) 71–176.

[9] M.M. Shah, A general correlation for heat transfer during film condensation inside pipes, Int. J. Heat Mass Transfer 22 (1979) 547–556.

[10] A. Cavallini, R. Zecchin, A dimensionless correlation for heat transfer in forced convective condensation, Proceedings of the Fifth International Heat Transfer Conference, Japan Society of Mechanical Engineers 3 (1974) 309–313.

[11] D.B. Bivens, A. Yokozeki, Heat Transfer Coefficients and Transport Properties for Alternative Refrigerants, International Refrigerant Conference Proceedings, Purdue University, 1994.

[12] L. Tang, Empirical Study of New Refrigerant Flow Condensation Inside Horizontal Smooth Tube and Micro-Fin Tubes, Ph.D. Thesis, University of Maryland at College Park, 1997.

[13] E.F. Carpenter, A.P. Colburn, The effect of vapor velocity on condensation inside tubes, Proc. Gen. Dis. Heat Transfer (1951) 20–26.

[14] H.M. Soliman, J.R. Schuster, P.J. Benson, A general heat transfer correlation for annular flow condensation, J. Heat Transfer 90 (1968) 267–276.

[15] S.L. Chen, F.M. Gerner, C.L. Tien, General film condensation correlations, Exp. Heat Transfer 1 (1987) 93–107.

[16] D.P. Traviss, W.M. Rohsenow, A.B. Baron, Forced convective condensation in tubes: a heat transfer correlation for condenser design, ASHRAE Trans. 79 (1) (1973) 157–165.

[17] E.T. Hurlbert, T.A. Newell, Characteristics of refrigerant film thickness, pressure drop, and condensation heat transfer in annular flow, HVAC&R Res. 5 (3) (1999) 29–247.

[18] H. Haraguchi, S. Koyama, T. Fujii, Condensation of refrigerants HCFC 22, HFC 134a, and HCFC 123 in a horizontal smooth tube (2nd report, proposal of empirical expressions for local heat transfer coefficient), Trans. JSME 60 (574) (1994) 245–252.

[19] H.M. Soliman, On the annular-to-wavy flow pattern transition during condensation inside horizontal tubes, Can. J. Chem. Eng. 60 (1982) 475–481.

[20] A. Cavallini, G. Censi, D. Del Col, L. Doretti, G.A. Longo, L. Rossetto, C. Zilio, In-tube condensation of halogenated refrigerants, ASHRAE Trans. 108 (1) (2002) 146–161.

[21] J.R. Thome, J. El Hajal, A. Cavalini, Condensation in horizontal tubes, part 2: new heat transfer model based on flow regimes, Int. J. Heat Mass Transfer 46 (2003) 3365–3387.

[22] D. Steiner, Heat transfer to boiling saturated liquids, VDI-Wärmeatlas (VDI Heat Atlas), Verein Deutscher Ingenieure, VDI-Gesellschaft Verfahrenstechnik und Chemieingenieurwesen (GCV), Düsseldorf (1993), Chapter Hbb.

[23] J. El Hajal, J.R. Thome, A. Cavalini, Condensation in horizontal tubes, part 1: two-phase flow pattern map, Int. J. Heat Mass Transfer 46 (2003) 3349–3363.

[24] N. Kattan, J.R. Thome, D. Favrat, Flow boiling in horizontal tubes: part 1 – development of a diabatic twophase flow pattern map, J. Heat Transfer 120 (1998) 140–147.

[25] A. Cavallini, G. Censi, D. Del Col, L. Doretti, G.A. Longo, L. Rossetto, C. Zilio, Condensation inside and outside smooth and enhanced tubes – a review of recent research, Int. J. Refrigerat. 26 (4) (2003) 373–392.
[26] Y. Taitel, A.E. Dukler, A model for predicting flow regime transitions in horizontal and near horizontal gas-liquid flow, Am. Inst. Chem. Eng. J. 22 (1) (1976) 47–55.
[27] J.W. Coleman, S. Garimella, Two-phase flow regimes in round, square and rectangular tubes during condensation of refrigerant R134a, Int. J. Refrigerat. 26 (2003) 117–128.
[28] V.G. Niño, Characterization of Two-phase Flow in Microchannels, Ph.D. Thesis, University of Illinois, Urbana-Champaign, IL, 2002.
[29] J.M. Mandhane, G.A. Gregory, K. Aziz, A flow pattern map for gas-liquid flow in horizontal and inclined pipes, Int. J. Multiphase Flow 1 (1974) 537–553.
[30] E.W. Jassim, T.A. Newell, J.C. Chato, Probabilistic determination of two-phase flow regimes utilizing an automated image recognition technique, Exp. Fluid. 42 (2007) 563–573.
[31] M.K. Dobson, Heat Transfer and Flow Regimes During Condensation in Horizontal Tubes, Ph.D. Thesis, University of Illinois, Urbana-Champaign, IL, 1994.
[32] P.S. Sacks, Measured Characteristics of Adiabatic and Condensing Single Component Two-Phase Flow of Refrigerant in a 0.377 in. Diameter Horizontal Tube, ASME Winter Annual Meeting, 75-WA/HT-24 Houston, Texas, 1975.